A pulse-compression-ring circuit for high-efficiency electric propulsion

Thomas L. Owens[a)]
West Virginia High Technology Consortium Foundation, 1000 Galliher Drive, Fairmont, West Virginia 26554, USA

(Received 27 November 2007; accepted 1 January 2008; published online 6 March 2008)

A highly efficient, highly reliable pulsed-power system has been developed for use in high power, repetitively pulsed inductive plasma thrusters. The pulsed inductive thruster ejects plasma propellant at a high velocity using a Lorentz force developed through inductive coupling to the plasma. Having greatly increased propellant-utilization efficiency compared to chemical rockets, this type of electric propulsion system may one day propel spacecraft on long-duration deep-space missions. High system reliability and electrical efficiency are extremely important for these extended missions. In the prototype pulsed-power system described here, exceptional reliability is achieved using a pulse-compression circuit driven by both active solid-state switching and passive magnetic switching. High efficiency is achieved using a novel ring architecture that recovers unused energy in a pulse-compression system with minimal circuit loss after each impulse. As an added benefit, voltage reversal is eliminated in the ring topology, resulting in long lifetimes for energy-storage capacitors. System tests were performed using an adjustable inductive load at a voltage level of 3.3 kV, a peak current of 20 kA, and a current switching rate of 15 kA/μs. © *2008 American Institute of Physics.* [DOI: 10.1063/1.2836329]

I. INTRODUCTION

One of the principal advantages of electric propulsion for space travel is the highly efficient utilization of the propellant supply, which results from the relatively high velocities imparted to the propellant mass as it is ejected from the spacecraft.[1] Compared to chemically propelled spacecraft, the reduction in propellant supply afforded by electric propulsion allows a greater fraction of the spacecraft to be occupied by useful payload. While electric propulsion systems reduce the amount of propellant that must be carried on-board a spacecraft, they have very low thrust compared to chemical thrusters. Consequently, electric propulsion systems are well suited to missions that require large changes or frequent changes in spacecraft velocity over long periods of time. For example, missions that involve long-range space travel, frequent satellite repositioning, or satellite station keeping would be good candidates for electric propulsion.

There are at least three general approaches to electric propulsion, including electrothermal, electrostatic, and electromagnetic systems.[1] The pulsed-power system described in this paper is designed for electromagnetic thrusters. There are currently two general types of electromagnetic thrusters, both of which use a Lorentz force to eject plasma propellant at high velocity. The first type of thruster creates the Lorentz force by driving plasma current between planar or annular conductive electrodes that are in direct contact with the plasma.[1] This type of thruster can be operated continuously or in a pulsed mode.[2] In general, direct plasma contact leads to excessive electrode erosion at high power levels, which limits the operational life of the thruster. Erosion problems have been alleviated through the use of lithium-fed multichannel hollow cathodes and lithium propellant,[3] but this solution restricts the range of propellants that may be supplied to the thruster.

The second type of electromagnetic thruster eliminates electrode contact by coupling to the plasma inductively across a thin insulating barrier.[1,4,7] Inductive thrusters are inherently pulsed devices, whose repetitive, high-current operation complicates the power supply design compared to steady-state plasma thrusters. One of the primary attractions of inductive thrusters is the elimination of contact electrodes, which mitigates issues with material erosion. The elimination of contact electrodes allows the use of a wide range of propellants, which might otherwise oxidize or enhance the erosion of conducting electrodes. In particular, a number of common on-board propellants or propellants derived from *in situ* resources may be used. For example, water derived from lunar or Martian ice has been suggested as a potential *in situ* source of propellant for inductive thrusters. By avoiding plasma contact with metal electrodes, the instantaneous thruster power can be increased well beyond levels where damage would occur in steady-state electromagnetic thrusters, allowing relatively high levels of thrust to be sustained for long periods of time. Thrust levels can be adjusted by changing the pulse repetition period, while maintaining high plasma exhaust velocity and high thruster efficiency.

Electric thrusters must have high electrical efficiency in order to minimize the size and weight of the thruster and its associated power source. Electric thrusters must also be sufficiently robust to endure the rigors of space without maintenance. The pulse-compression-ring system described in this document was developed with these requirements in mind. A single-stage embodiment of this concept will be

a)Electronic mail: towens@wvhtf.org.

tested on an experimental pulsed inductive thruster[5] patterned after the FARAD device developed at Princeton University.[6] The principal element of the thruster is a flat coil composed of a pattern of six interleaved two-turn spiral coils arranged around a circle. The coil configuration is similar to, but smaller than, the PIT MkV coil used by Dailey and Loveberg in their pioneering work in inductive electric propulsion.[7] The FARAD thruster adds a preionizer which greatly reduces the peak voltage needed to start the main plasma discharge. The preionizer consists of a vector inversion generator that applies a short burst of radio-frequency energy to the propellant gas at the beginning of each pulse.[5]

As will be described in Sec. II, the novel pulse-compression-ring architecture developed for this experimental thruster has an improved energy efficiency and lifetime compared to conventional pulse-compression systems. The system also has a number of features in common with conventional pulse-compression systems. For example, solid-state switching in the pulse-compression ring is carried out prior to pulse compression, while the pulse duration is relatively long and the current level is low. This procedure maintains electric current and rate of rise of current (di/dt) within the rating of many common solid-state switches. Pulse compression transforms the relatively low-current, long-duration pulses formed by the active switches into pulses with much higher peak currents and di/dt levels at the load.

With sufficient pulse compression in a typical thruster, electric current and di/dt at the solid-state switch can be made low enough that commercial insulated-gate bipolar transistor (IGBT) switches may be used. IGBT switches are relatively fast solid-state switches that can provide high pulse-repetition rates without sacrificing peak-power capability. Since the size and weight of the pulsed-power system are determined primarily by energy per pulse rather than pulse rate, high repetition rates will lead to low spacecraft alpha (kg/kW), as well as high average power and average thrust. As will be described in the next section, the use of pulse compression allows extremely high-current switching in the output stage through the use of passive saturable inductors, sometimes known as magnetic switches. More significantly, these passive magnetic switches can tolerate the extremely high di/dt levels required for efficient thruster performance.

II. PULSE-COMPRESSION-RING ARCHITECTURE

In conventional pulse compression systems,[8–11] a series of inductors and capacitors are interconnected to form a chain of resonant-transfer circuits. A pulse at the beginning of the chain is compressed in time and increased in amplitude as the time constants of successive resonant-transfer blocks decrease along the chain. A topological separation exists between the input and the output ends of this distributed circuit. Pulse energy can travel in both directions along the in-line chain of circuit elements.

If the plasma load in an electric thruster presents an impedance mismatch to the pulse-compression circuit, only a portion of the incident pulse energy is coupled into the plasma, where it provides plasma acceleration and heating. The remaining energy is reflected from the load and sent back toward the input end of the circuit. Reflected energies on the order of 50% of the incident energy are common for inductive plasma thrusters.[4] After traveling back through the entire compression chain, some of the reflected energy can be recovered at the input end of the system in a special fly-back circuit.[9] However, circuit losses along the return path absorb significant energy for large mismatches, which reduces overall-system efficiency.

Furthermore, the reflected pulse is inverted from the incident pulse, which shortens capacitor lifetime by the empirically derived factor,[12]

$$f = \left[\frac{\ln(R_o)}{\ln(R)}\right]^{-q}, \tag{1}$$

where R is the voltage-reversal fraction (voltage reversal divided by the capacitor voltage rating), R_o is the rated-voltage-reversal fraction for the capacitor, and q is an experimentally determined exponent. A common capacitor used in tests described in Sec. IV has $q \sim 2.2$ and $R_o \sim 0.2$. In this case, a 50% voltage reversal reduces capacitor lifetime by a factor of 6, representing a substantial decrease in lifetime.

The problem with energy efficiency in conventional in-line pulse compression circuits can be overcome by recovering unused energy promptly at the load before it propagates back through a large number of lossy circuit elements. Prompt energy recovery at the load is accomplished by connecting the output end of the circuit directly to the input end so that current which passes through the load coil flows immediately into the capacitor at the electrical input of the line. Energy is held in the input capacitor using a steering diode in the last stage of the pulse-compression chain. The steering diode forces energy circulation in one direction only. In effect, a pulse-compression ring is formed that maintains energy flow in one direction around the ring, without reflection.

Since energy flows in only one direction and there is no reflection, there is no voltage reversal on any of the energy-storage capacitors in the system. With no voltage reversal, the lifetime of energy-storage capacitors is greatly extended compared to lifetimes in conventional in-line pulse-compression systems, as described in connection with Eq. (1). Long-life components are critically important for long-duration space missions where maintenance and repair are infeasible.

PSPICE simulations. Figure 1 is a PSPICE circuit schematic showing one embodiment of the pulse-compression-ring concept. In this case, a 100 J system is depicted that is designed for the aforementioned FARAD prototype electric thruster.[5] The principal compression elements consist of capacitors (C1, C2, and C3), saturable inductors (L10, L2, and L3), and fixed air-core inductor (L1). The cores of the saturable inductors are composed of Metglas®, which has a saturated magnetic field of approximately 1.6 T. Magnetic properties of the saturable inductor cores are captured in PSPICE using a Jiles-Atherton model with hysteresis data supplied by the manufacturer of the Metglas® cores.

In the present context, saturable inductors act as switches since they present high impedance to current flow when the inductor cores are unsaturated and a low impedance to current flow when the cores become saturated. The

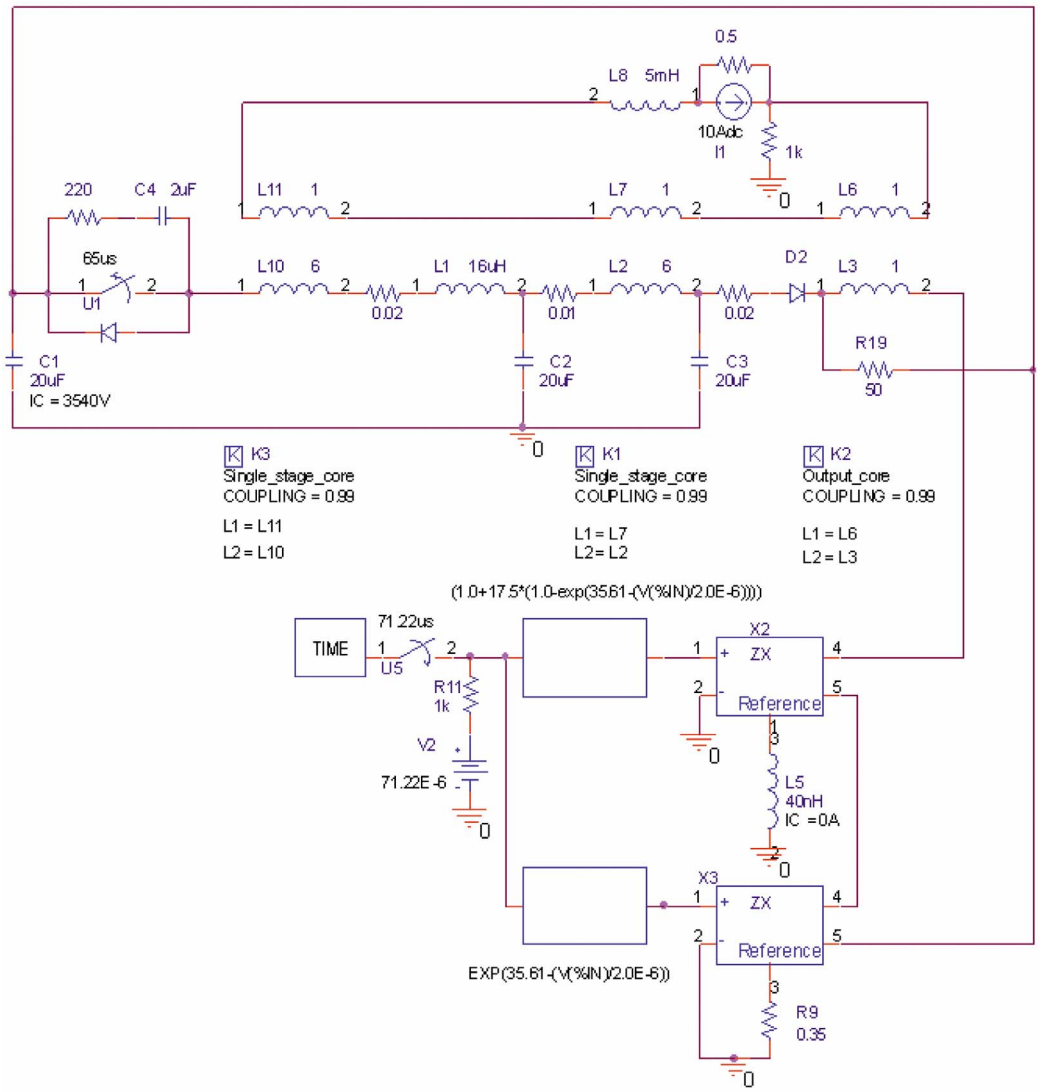

FIG. 1. (Color online) Schematic diagram of a 100 J pulse-compression-ring circuit.

unsaturated state of the cores is analogous to an open-circuited switch, while the saturated state of the cores is analogous to a closed switch. Because of the analogy to ideal switches, the saturable inductors are sometimes referred to as magnetic switches. The change in state from an unsaturated core to a saturated core is brought about by the application of sufficient volt-seconds at the inductor terminals, according to the integral form of Faradays law,

$$\int Vdt = 2nA_cB_s, \tag{2}$$

where n is the number of conductor turns around the core, A_c is the cross-sectional area of the core, and B_s is the saturated magnetic field of the core. Thus, after voltage on C1 provides sufficient volt-seconds to drive inductor L1 into saturation, essentially all of the charge from C1 flows into C2 in a resonant transfer of energy between identical capacitors. Similarly, when sufficient volt-seconds are applied to saturable inductor L2, there is a complete transfer of energy from C2 to C3. The saturated inductance of L2 is designed to be less than the saturated inductance of L1 so that the second resonant transfer is faster than the first resonant transfer, leading to foreshortening of the pulse. Since electric charge is conserved during each transfer, the compressed current increases by the same factor by which the pulse duration decreases.

In the output stage of the pulse-compression circuit, saturable inductor L3 acts as a final magnetic switch between the output capacitor C3 and the load. Since the pulse has been compressed at this point without changing the voltage level, low volt-seconds are applied to the output switch. Low volt-seconds allow a reasonably small core cross section to help reduce the mass of the final magnetic switch in accordance with Eq. (2). If the load inductance is less than the saturated inductance of the output magnetic switch, additional pulse compression will take place in the output circuit, making the device, in effect, a two-stage compressor.

To simulate plasma acceleration from an inductive coil, the load is modeled as a resistor R3, in series with a time varying inductor. The time dependence of the load inductor is given by an empirical formula,[7]

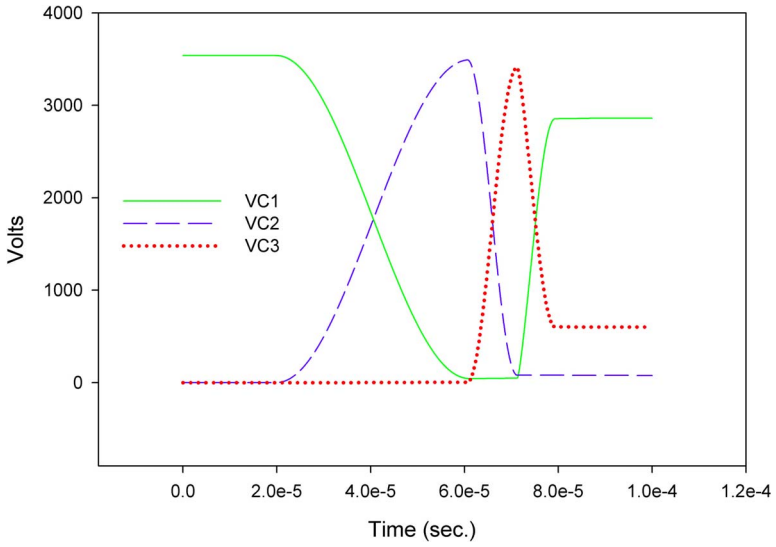

FIG. 2. (Color online) Capacitor voltage waveforms in the 100 J pulse-compression-ring circuit obtained from PSPICE simulations.

$$L = L_e + L_c\left[1 - \exp\left(-\frac{t}{\tau}\right)\right], \tag{3}$$

where L_e represents the inductance in the coil leads, L_c is the free-space inductance of the coil, and τ is the characteristic time period over which plasma acceleration takes place. This load is formed in PSPICE using analog behavioral models connected between the magnetic switch L3 and the input capacitor C1, as shown in Fig. 1.

The output capacitor C3 is connected to the input capacitor C1 via the magnetic switch L3, diode D2, and the simulated plasma load. With this arrangement, the energy that is not dissipated in the load is recovered in the input capacitor C1. A circular path for energy flow is created, forming, in effect, a pulse-compression ring. In contrast to the conventional in-line pulse-compression systems described in Refs. 8–11, the energy in the pulse-compression ring makes only a single transit through the circuit. Minimizing the pulse-propagation path in this way reduces circuit loss substantially, given the large pulse reflections that typically occur in electric propulsion systems. In addition, pulse propagation in a single pass eliminates voltage reversal on all of the energy-storage capacitors in the pulse-compression ring, greatly extending capacitor lifetime compared to conventional systems, as described previously.

In the hardware implementation, solid-state switch U2 is actually formed from an array of eight IGBTs in order to handle large switching currents. The emitter of each IGBT is connected to a separate coil wrapped around a common core that makes up inductor L10. After triggering the IGBTs, the current flow is held off for several microseconds by the unsaturated core of L10 to allow enlargement of the effective-internal-conduction area of the IGBTs. Switching losses in the IGBTs are thereby held to a minimum, while di/dt capability is maximized. After L10 saturates, current flows simultaneously in all eight IGBTs, even if there are differences in the trigger signals to each IGBT. Equal division of current at this point is assured by equalizing the saturated inductances in series with each IGBT. The control of switching characteristics by the above means is sometimes referred to as magnetic assist.

In a similar manner, magnetic assist is provided for the output diode D2 through the magnetic switch L3. In the hardware implementation, diode D2 consists of an array of six individual diodes connected in parallel. The cathode of each diode is connected to a separate conductor which wraps around the core of the magnetic switch L3. The diodes become forward conducting a few microseconds before the core of the magnetic switch L3 saturates. The brief hold-off period before L3 saturates results in reduced losses in the diode and increased di/dt capability, just as it did for the IGBT switches.

Figure 2 shows the voltage waveforms, calculated using PSPICE, at each capacitor in the pulse-compression ring depicted in Fig. 1. Figure 3 shows the corresponding capacitor current waveforms. It is evident in these figures that the capacitor voltages are always positive, leading to increased capacitor lifetimes, as described previously. Figure 2 also shows voltage recovery in the initial capacitor C1 near the end of the pulse. For the assumed resistive losses in this PSPICE example, approximately 64% of the initial energy is recovered at the end of the pulse cycle, with most of the energy lost to plasma acceleration, simulated in PSPICE through the time varying load inductance given by Eq. (2).

In Fig. 2, a small amount of charge remains in C3 after the energy has been recovered in C1 at the end of the pulse cycle. This unutilized charge can be scavenged for use in other parts of the spacecraft (e.g., to charge batteries), but it is not easily recovered within the pulsed-power train. In the present example, this charge is drained between pulse cycles, resulting in an additional energy loss in the system. Energy lost by this means is typically very small, representing only 2% of the initial energy in the present example. Immediately after plasma formation at the face of the load coil, the initial coil inductance drops well below its free-space value. When the plasma has accelerated away from the load coil, the coil inductance returns to its free-space value. For the simulation

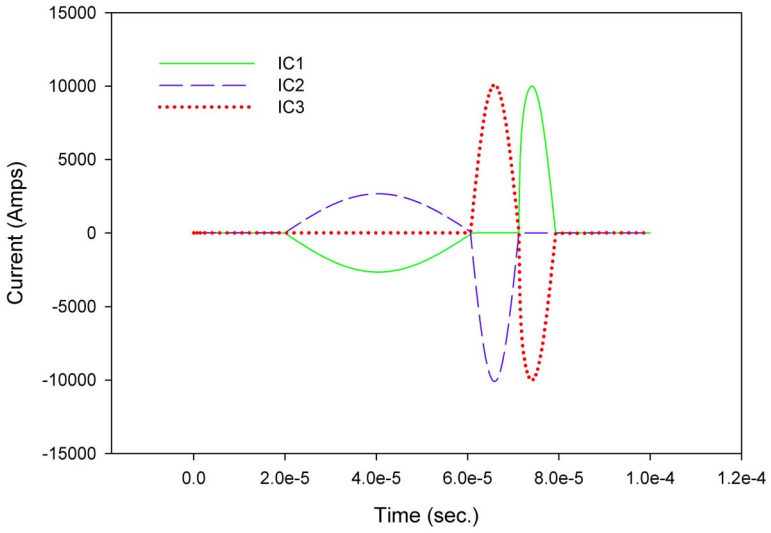

FIG. 3. (Color online) Capacitor current waveforms in the 100 J pulse-compression-ring circuit obtained from PSPICE simulations.

results shown in Figs. 2 and 3, the coil inductance immediately after plasma formation is assumed to be 40 nH, dropping to a free-space value of 700 nH after the plasma has been ejected. Combining this load coil inductance with the magnetic switch inductance L3, the calculated current-rate-of-rise (di/dt) in the load coil becomes approximately 30 kA/μs. Lower di/dt values are found in the hardware tests described in Sec. IV due to larger values of initial inductance in the load coil.

The design presented in Fig. 1 was selected to allow the use of available in-house components. In a straight-forward manner, multiple compression stages may be used with lower gain per stage, but higher overall-system gain. With increased overall-compression gain, the current through the primary solid-state switches is reduced and fewer parallel IGBT switches are required. With lower compression gain per stage, the size and weight of magnetic switch cores may be reduced substantially, since switch core size is proportional to the square of compression gain.[8] Parametric studies using PSPICE indicate that a three-stage device would be optimal with respect to overall-system mass, but this optimization was not attempted in the present study due to limited project costs and the need to use available in-house components. Since the primary goal of this effort was to demonstrate the benefits of the pulse-compression-ring circuit to improve thruster electrical efficiency, the mass optimized design has been left for future work.

III. HARDWARE IMPLEMENTATION

Figure 4 is a diagram of the hardware implementation of the 100 J pulse-compression ring depicted schematically in Fig. 1. As mentioned in the last section, eight IGBT switches are connected in parallel for primary switching prior to compression. Eight IGBT switches are needed in order to handle, conservatively, a peak current of 2.8 kA at 3600 V, calculated in the PSPICE simulations, as displayed in Figs. 2 and 3. The IGBTs are arranged in a circle about the axis of the assembly shown in Fig. 4 to match the cylindrical geometry of the load coil. Optical triggering of the IGBTs provides complete electrical isolation of the trigger circuit. The emitter of each IGBT is connected to an individual six-turn coil surrounding the magnetic-assist core L10, which assures that all IGBTs conduct equal currents simultaneously and energy

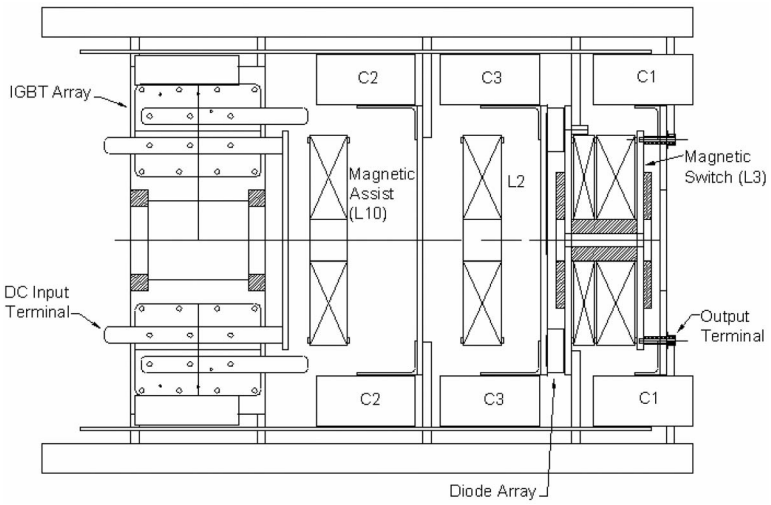

FIG. 4. Hardware design of the 100 J pulse-compression-ring system.

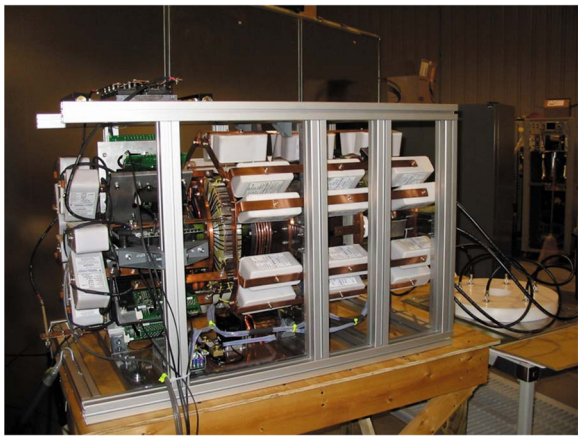

FIG. 5. (Color online) Photograph of the completed 100 J pulse-compression-ring system.

loss in the IGBTs is minimized. Three 20 μF capacitor banks (C1, C2, and C3) are assembled from 30 individual 2 μF capacitors rated at 5 kV each.

A circular array of six equally spaced terminals at the right end of the assembly feed power to the induction coil (not shown) that would be connected at the right end of the assembly. The coil is formed from a set of six individual spiral windings as described in Ref. 5. Capacitors are arranged in a circle surrounding the toroidal inductor cores. This configuration results in a compact assembly that maintains the cylindrical geometry needed for uniform current flow in the circular array of terminals which connect to the load coil.

The single magnetic switch L3 shown in Fig. 1 at the output end of the assembly actually consists of six independent single-turn magnetic switches formed around a common core. Each of the six magnetic switches connects to an individual diode. The six diodes in this array are depicted in Fig. 1 by the single diode D2. While even a single diode in the array can handle a peak current of approximately 10 kA, six parallel diodes are required to accommodate the large di/dt. As mentioned previously, the magnetic switch L3 doubles as a magnetic assist for the diode array, which equalizes current division among the diodes, increases di/dt capability, and minimizes energy loss in the diodes.

The input capacitor C1 is located very close to the inductive thruster coil at the output end of the power train to minimize lead resistance and lead inductance for maximum energy recovery in C1. While lead resistance and lead inductance from the load coil to C1 are minimized in this configuration, a relatively large inductance exists in the long conduction path from C1 back to the IGBT switch array. A large stray inductance in this path is not a problem, since it merely adds to the inductance of the air-core inductor L1 in the first stage of the pulse-compressor chain. The total inductance of these elements in series with capacitors C1 and C2 determines the initial period of the pulse and the peak current through the IGBTs prior to pulse compression.

Figure 5 is a photograph of the completed pulse-compression-ring system. A side view of the device is shown in the photograph similar to the view depicted in Fig. 4. The circular IGBT array is visible near the left end of the assembly, and the three energy-storage capacitor banks are seen to the right of the IGBT array. The capacitors arranged in a circle at the extreme left of the unit form part of a transient suppressor circuit around the IGBTs that will be described in the next section. The bias circuitry for the magnetic switch cores is located on a platform at the bottom of the assembly. The bias circuit consists of a small dc power supply, a series inductor, and a current shunt. The whole assembly is mounted within an aluminum frame that measures approximately 1.0 m long, 0.7 m high, and 0.7 m wide.

IV. TEST RESULTS

In anticipation of testing plasma acceleration in an experimental inductive thruster,[5] the pulse-compression-ring system was discharged into a load consisting of a spare induction coil operated in the open air. The coil assembly was identical to the assembly that will be used in the plasma acceleration experiments. The conductors forming the principal coil elements were embedded within an epoxy compound that, in turn, was encapsulated within a polyethylene disk. The complete coil assembly is shown in lower-right portion of the photograph in Fig. 5, with the plane of the coil lying horizontally on a table next to the pulse-compression ring. Six coaxial cables connect the pulse-compression-ring output connectors to the six input terminals of the coil. A moveable aluminum plate was placed in front of the coil to approximate the effect of high-conductivity plasma at various fixed positions in front of the coil. For some of the tests, the plate was placed tight against the face of the coil assembly to obtain the minimum coil inductance, thereby simulating the high di/dt situation that occurs as the plasma forms in front of the coil.

Figure 6 shows the experimental voltage waveforms produced in energy-storage capacitors C1, C2, and C3 during a pulse-compression cycle. In this case, the initial charge on the first energy-storage capacitor C1 was about 3.3 kV, corresponding to an initial stored energy of 109 J. In qualitative agreement with the PSPICE simulations, voltage in the first capacitor in the chain is held for several microseconds until the first inductor L1 saturates. Capacitor C1 then discharges into the second capacitor C2 in a resonant transfer of energy. Voltage is held in capacitor C2 until inductor L2 saturates. Energy is then resonantly transferred to capacitor C3. Finally, when inductor L3 saturates, capacitor C3 discharges through the induction coil back into the first capacitor (C1) in the chain. Since the saturated inductance decreases along the chain while the capacitance remains constant, the period of the pulses decreases as the pulse propagates through the circuit. Energy not dissipated in the load coil or in circuit losses is recirculated back into capacitor C1, where it is held using diode array D2. After make-up charge is added to capacitor C1, the system is ready for the next pulse.

A transient is observed in the voltage on C1 as energy is recovered near the end of the pulse [Fig. 6(a)]. This transient is due to the intrinsic properties of the power diodes as they transition from a forward-biased condition to a reverse-biased condition. During this short transition period, charge

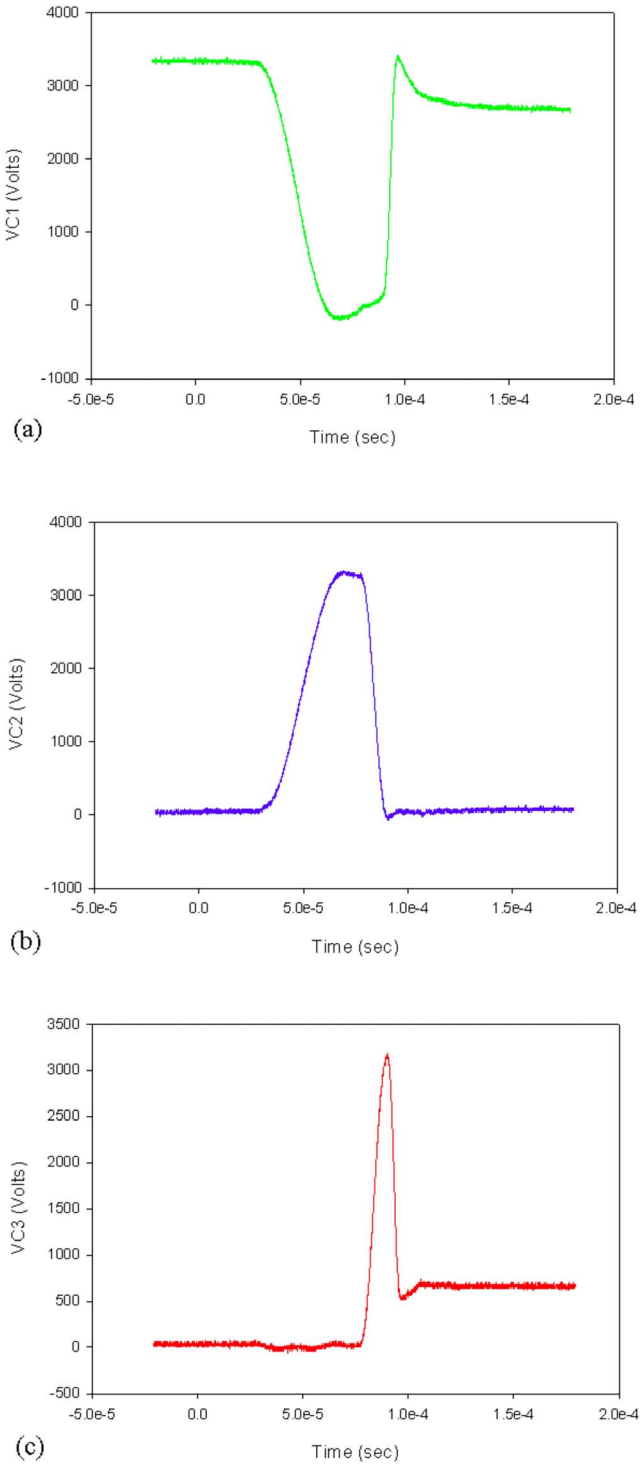

FIG. 6. (Color online) Measured voltage waveforms in energy-storage capacitors C1, C2, and C3 of the experimental pulse-compression ring.

carriers are drained from the internal drift region of the diode followed by a build up of space charge in the diode depletion layer.[13] These processes result in a small negative excursion of the diode current after the much larger positive current has discharged through the diode into capacitor C1. This small negative excursion is evident in the test measurements shown in Figs. 7 and 8. It is this negative current transient that reverses the time derivative of the voltage on capacitor C1, leading to the transient voltage peak in Fig. 6(a).

From the experimental data in Fig. 6, it is found that approximately 6% of the initial energy is lost in the IGBT switches and in hysteresis and Ohmic losses in the magnetic assist L10. Another 6% of the initial energy is dissipated in hysteresis losses in the second magnetic switch L2 and in Ohmic losses in the conductors and interconnections. Approximately 24% of the initial energy is dissipated in the output circuit, which includes the diode array, the magnetic switch L3, and the experimental induction coil that will eventually serve as the plasma power coupler. Included in the 24% energy loss is the energy dissipated in draining the remnant charge on C3. The energy lost by draining this charge is about 3% of the initial energy. As mentioned in Sec. II, the energy in the remnant charge on C3 can be scavenged between pulses for use in other parts of the spacecraft. All of the remaining energy, equal to 64% of the initial energy, is recovered in the system through the recirculating-ring topology.

Manufacturer's data for the IGBT switches indicate that at least 18% of the initial energy would normally have been lost in the IGBTs alone if they switched the applied current at the applied voltage. IGBT losses are far lower than 18% because switching occurs at zero current in the present design, and the magnetic assist L10 holds off most of the current through the IGBTs until their internal impedance drops to a value approaching the steady-state value.

Figure 7 shows the current in the return path between capacitors C1 and C3. The first negative peak is the current through the IGBT switches, while the second positive peak is the current through the load coil. In close agreement with the PSPICE simulations, the peak current through the IGBTs is 2.9 kA and the pulse period is 40 μs. Compressed current passing though the load coil reaches a peak of approximately 15 kA. The rate of current rise in the coil at the beginning of the pulse is about 8 kA/μs. The rate of rise in this case is constrained by the maximum applied voltage and the minimum inductance in the circuit loop containing the load coil. Measured inductances in this loop were the following: load coil minimum ~200 nH, magnetic switch ~55 nH, coaxial leads ~55 nH, and capacitors ~30 nH.

The load coil inductance shown above is a minimum, since it was obtained with an aluminum plate resting against the face of the coil assembly. Inductance is finite in this situation since there is a layer of insulation between the coil conductors and the face of the assembly.

In order to test higher di/dt levels, the output inductance needs to be reduced still further. This was accomplished by removing the load coil from the circuit and short circuiting the ends of the coaxial leads that were previously connected to the load coil. From the list of inductances shown above, the total output inductance presented to the pulse-compression ring then drops from 340 to 140 nH.

Figure 8 shows the resulting current with an applied voltage of 3 kV. In this case, a peak current of 20 kA flows through the load inductance. Figure 8(b) provides an expanded view of the positive peak in order to show the current rise time more clearly. In this case, di/dt is slightly greater than 15 kA/μs. This level exceeds the quoted maximum di/dt rating of the diodes by about 30%. As described in Sec.

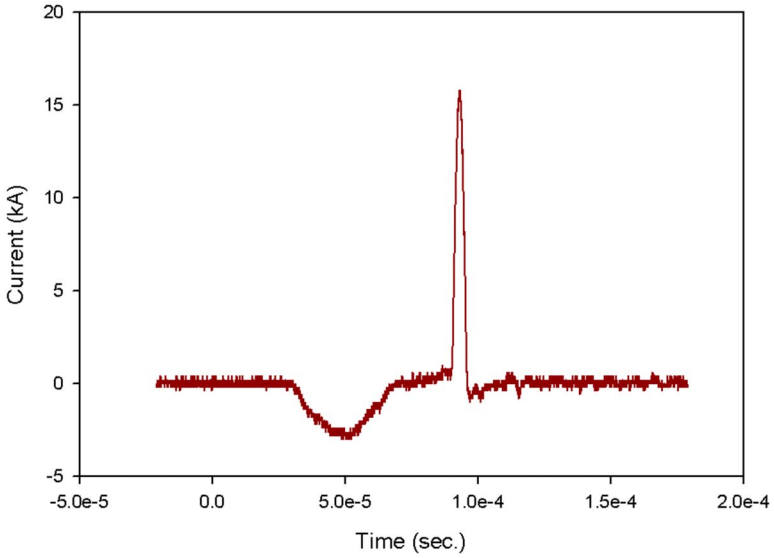

FIG. 7. (Color online) Measured current flow into the initial energy-storage capacitor C1 with minimum coil inductance and maximum di/dt through the load coil. The negative peak shows the measured current through the IGBT switches, and the positive peak shows the measured current through the load coil.

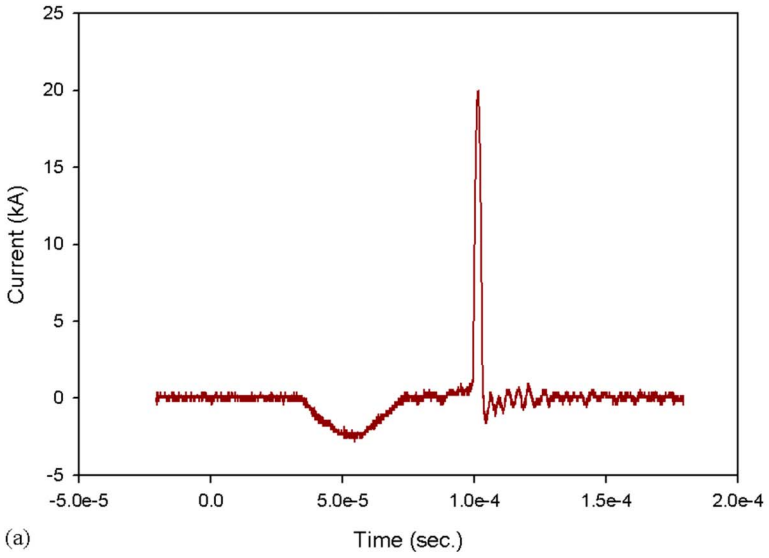

(a)

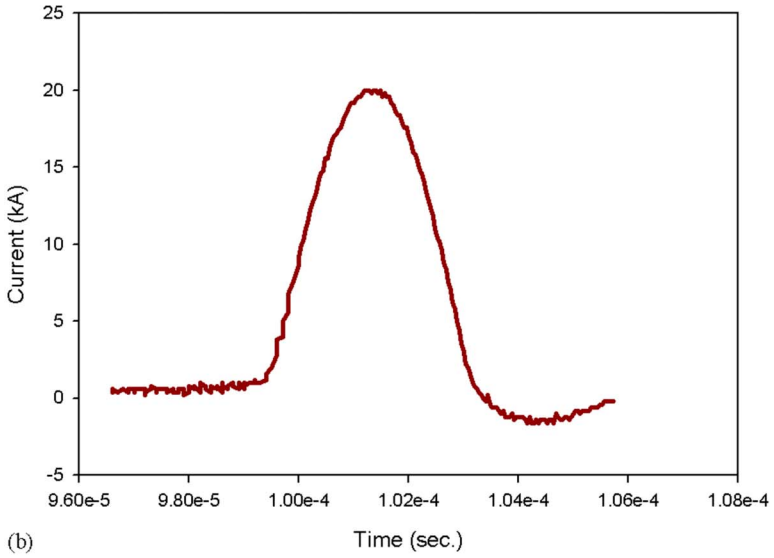

(b)

FIG. 8. (Color online) (a) Measured current flow into the initial energy-storage capacitor C1 with the load coil replaced by a short circuit that reduces the load inductance and increases di/dt. The negative peak shows the measured current through the IGBT switches and the positive peak shows the measured current through the load coil. (b) Magnified view of the measured current through the load.

II, by placing the diode array ahead of the output magnetic switch L3, the magnetic switch provides a magnetic assist for the diodes, which allows increased di/dt and reduced loss in the diodes. Since the system was not tested to destruction, the absolute upper limit on di/dt for the diode array with magnetic assist lies somewhere above the 15 kA/μs measured in these tests.

Transient suppression. Transient voltages develop across the solid-state elements of the pulse-compression ring that can severely limit performance or damage components if they are not adequately suppressed. One such transient develops across the IGBT switch array shortly after the basic pulse cycle has completed and the first energy-storage capacitor C1 has recovered unused energy. At this point in time, capacitor C1 applies volt-seconds to the saturable inductor L10 through the residual resistance of the reverse-biased IGBTs. This causes the core of inductor L10 to switch from one extreme of its hysteresis curve to the other. While there are only a few milliamps of current flowing through the inductor, the extremely large and rapid change in inductance in L10 produces a negative voltage transient of several kilovolts. With positive voltage on the collector side of the IGBT array, this negative voltage transient can easily produce a momentary voltage across the IGBTs exceeding the reverse-voltage-hold-off capacity of the IGBTs.

This transient can be effectively eliminated by placing a resistor and a capacitor across the IGBT collector and emitter, as shown in Fig. 1. This resistor/capacitor circuit not only suppresses any rapid changes in voltage, but it can also reduce the net volt-seconds applied to the saturated inductor L10 to the point that spurious magnetic switching does not take place. In the present case, a 2 μF capacitor in series with a 220 Ω resistor across each IGBT provides ample suppression of this transient.

A second transient develops across the diode array D2. This second transient is also associated with the change in state of a magnetic switch. In this case, output switch L3 changes state shortly after the input capacitor C1 has recovered unused energy and recharged at the end of the pulse cycle. After C1 recharges, it reverses the volt-seconds applied to the inductor L3, causing it to become conductive for current flow from C1 back though the load inductor. Because the diode array D2 is transitioning to a reverse-biased state, current flows into the diode array only transiently in order to charge the junction capacitance and drain the carriers in the diode array. A resonant circuit loop is formed consisting of the capacitor C1, the load switch inductors, and the diode junction capacitance. Since the diode junction capacitance is far less than the capacitance of C1, the voltage across the diode momentarily reaches twice the voltage on the input capacitor C1 as energy is resonantly transferred from C1. This transient can easily damage the diode array by exceeding the reverse-hold-off limit of the diodes.

This diode transient would normally be suppressed with a rc snubber network placed across the diode. The snubber network cannot be placed here because the snubber capacitor would be charged to a voltage equal to the dc supply voltage at the beginning of the pulse cycle via the return path connecting the load inductor to the initial energy-storage capacitor C1. With this initial voltage on the snubber capacitor, the cathode end of diode array would reach approximately twice the supply voltage when the input pulse reached capacitor C2.

Instead of placing a conventional snubber network across the diode array, the diode transient is suppressed by connecting a shunt resistor across the magnetic switch L3 and the load inductor, as shown in Fig. 1. The resistor has much larger impedance than the impedance of the output inductors that it shunts, so the resistor does not affect the pulse current through the load. Rather, the shunt resistor allows current flow from C1 to the cathode end of the diode array before the magnetic switch L3 reverses state. The diode junction capacitance then charges nonresonantly to the voltage level of capacitor C1. In this state, the voltage drop across the output inductors becomes zero and there is no resonant energy transfer from C1 to the junction capacitance and no damaging transient when the magnetic switch L3 changes state.

V. SUMMARY

A novel 100 J pulse-compression-ring circuit for inductive electric propulsion was successfully demonstrated. The design was motivated by the need for high electrical efficiency, low system-mass relative to power level, and long component lifetime on extended space missions. Test results demonstrated efficient excess energy recovery in the unique recirculating ring topology. The ring topology also eliminated voltage reversal across energy-storage capacitors, leading to substantially increased capacitor lifetime relative to conventional pulse-compression systems. In common with other pulse-compression systems, the pulse-compression ring allowed the use of fast IGBT switches that may be operated at high pulse-repetition rates, leading to high average power for a given system mass. The 100 J system will be applied to an experimental inductive thruster currently under development.

ACKNOWLEDGMENTS

This work was supported by Grant No. NNM06AA17G from the National Aeronautics and Space Administration, managed through the NASA Marshall Space Flight Center (COTR: Dr. Michael LaPointe). The load coil used in system tests was designed by Dr. Kurt Polzin of the Marshall Space Flight Center, and fabricated by Mr. Robert Miller and Dr. Frank Rose of Radiance Technologies, Inc. Dr. Michael Goodman of the WVHTCF and Dr. Frank Rose of Radiance Technologies, Inc. provided project leadership and many insightful discussions. Mr. Robert Ice of the WVHTCF managed component construction and system assembly.

[1] R. G. Jahn, *Physics of Electric Propulsion* (Dover, Mineola, New York, 2006).
[2] J. K. Ziemer and E. Y. Choueiri, Proceedings of the 25th International Electric Propulsion Conference, Cleveland, OH, 1997 (unpublished).
[3] V. P. Ageyev and V. G. Ostrovsky, Proceedings of the 23rd International Electric Propulsion Conference, Seattle, WA, 1993 (unpublished).
[4] A. Martin and R. Eskridge, J. Phys. D **38**, 4168 (2005).
[5] K. A. Polzin, M. F. Rose, R. Miller, S. Best, T. Owens, and J. Dankanich, Proceedings of the 43rd AIAA/ASME/SAE/ASEE Joint Propulsion

Conference, Cincinnati, OH, 2007 (unpublished).
[6] E. Y. Choueiri and K. A. Polzin, Proceedings of the 40th AIAA/ASME/SAE/ASEE Joint Propulsion Conference, Ft. Lauderdale, FL, 2004 (unpublished).
[7] C. L. Dailey and R. H. Loveberg, AIAA J. **10**, 125 (1972).
[8] D. L. Birx, E. J. Lauer, E. J. Reginato, L. L. Schmidt, and M. Smith, Lawrence Livermore Laboratory Report No. UCID-18831, 1980 (unpublished).
[9] D. L. Birx, P. P. Das, I. V. Fomenkov, W. N. Partlo, and T. A. Watson, US Patent No. 5,729,562 (31 October 1996).
[10] W. C. Nunnally, Los Alamos National Laboratory Report No. LA-8862-MS, 1982 (unpublished).
[11] P. W. Smith, *Transient Electronics* (Wiley, New York, 2002).
[12] General Atomics Engineering Bulletin Nos. 96–004, 2003 (unpublished).
[13] N. Mohan, T. M. Undeland, and W. P. Robbins, *Power Electronics, Converters, Applications and Design* (Wiley, New York, 2003).